Biosensors and Bioelectronics 24 (2009) 1937–1941

Contents lists available at ScienceDirect

Biosensors and Bioelectronics

journal homepage: www.elsevier.com/locate/bios

Controlled torque on superparamagnetic beads for functional biosensors

X.J.A. Janssen[a,*], A.J. Schellekens[a], K. van Ommering[b], L.J. van IJzendoorn[a], M.W.J. Prins[a,b]

[a] Eindhoven University of Technology, Eindhoven, The Netherlands
[b] Philips Research, Eindhoven, The Netherlands

ARTICLE INFO

Article history:
Received 24 June 2008
Received in revised form
12 September 2008
Accepted 24 September 2008
Available online 14 October 2008

Keywords:
Superparamagnetic beads
Controlled torque
Rotation
Functional biosensor
Magnetic moment
Nanoparticle size distribution

ABSTRACT

We demonstrate that a rotating magnetic field can be used to apply a controlled torque on superparamagnetic beads which leads to a tunable bead rotation frequency in fluid. Smooth rotation is obtained for field rotation frequencies many orders of magnitude higher than the bead rotation frequency. A quantitative model is developed, based on results from a comprehensive set of experiments at different field strengths and frequencies. At low frequencies (<10 Hz), rotation is due to a small permanent magnetic moment in the bead. At high frequencies (kHz–MHz), the torque results from a phase lag between the applied field and the induced magnetic moment, caused by the non-zero relaxation time of magnetic nanoparticles in the bead. The control of torque and rotation will enable novel functional assays in bead-based biosensors.

1. Introduction

Particles with a nanometer to micrometer sizes are widely used as carriers and labels in bio-analytical systems (Mornet et al., 2004; Wild, 2005; Pollert et al., 2007). An important class of particles used in in-vitro diagnostics are so-called superparamagnetic beads, which consist of magnetic nanoparticles embedded inside a non-magnetic matrix (Fonnum et al., 2005). Superparamagnetic beads are powerful because they can be manipulated and detected inside complex biological fluids. Magnetic beads can for example be detected by magneto-resistive sensors (Baselt et al., 1998; Rife et al., 2003; Wirix-Speetjens et al., 2006; de Boer et al., 2007; Megens et al., 2007; Prins and Megens, 2007), Hall sensors (Besse et al., 2002; Ejsing et al., 2004, 2005; Fukumoto et al., 2005; Aytur et al., 2006), field coils (Astalan et al., 2004; Nikitin et al., 2007), and by optical detection (Mulvaney et al., 2007; Morozova and Morozov, 2008; Cohen-Tannoudji et al., 2008). These magnetic-label biosensors employ the magnetic beads as labels in order to measure the concentration of target molecules in a biological sample. We are investigating a novel generation of biosensors – called functional biosensors – in which the concentration as well as a functional property of biological molecules can be determined (Janssen et al., 2008). The principle of the biosensor is that a functional property of captured molecules is unveiled by measuring the response of magnetic beads to an electromagnetic actuation field. In an earlier publication we focused on the translational manipulation of single magnetic beads on a chip surface (Janssen et al., 2008). A complementary way to probe biological molecules is by applying a controlled torsion, i.e. a controlled rotation under well-defined torque. Bead-based single-molecule experiments, using low frequency (Hz) rotating magnetic fields, already indicate novel types of assays enabled by the application of rotation to biological molecules (Besteman et al., 2007; Koster et al., 2007). Although the degree of rotation was known in these single-molecule experiments, the quantitative value of the applied torque was not controlled. In fact, it is a surprise that a torque can be applied because in an idealized superparamagnetic bead the angle difference between the magnetization and the applied magnetic field is zero and thus the torque should be zero as well. This raises the question which physical mechanism is responsible for torque generation and how the magnitude of the torque depends on the magnitude and frequency of the applied rotation field. Applying high frequency (MHz) magnetic fields on ferrofluids has shown that the rotation of the magnetic moment and/or physical rotation of the nanoparticles depends on the strength of the field (Kurlyandskaya et al., 2003).

In this paper, we show how a well-defined torque can be applied on superparamagnetic beads, which consist of a large number of magnetic nanoparticles. We unravel the mechanisms of torque gen-

* Corresponding author at: Eindhoven University of Technology, Department of Applied Physics, NLaag f 1.10, P.O. Box 513, NL-5600 MB Eindhoven, The Netherlands. Tel.: +31 40 247 4663; fax: +31 40 247 2598.
E-mail address: x.j.a.janssen@tue.nl (X.J.A. Janssen).

0956-5663/$ – see front matter © 2008 Elsevier B.V. All rights reserved.
doi:10.1016/j.bios.2008.09.024

eration by a comprehensive set of experiments at different field strengths and frequencies, including field frequencies many orders of magnitude higher than the bead rotation frequency. We develop a quantitative model to calculate the torque on superparamagnetic beads and we discuss the application of torque control in functional biosensors.

2. Materials and methods

The magnetic beads used in this paper (Dynal M280, diameter 2.8 μm) consist of a composite material of non-uniform iron oxide nanoparticles (magnetite) in a polystyrene matrix. The purchased solution was diluted 4000 times in de-ionized water. A droplet of the solution was placed on a silicon chip, having crossed integrated current wires that create the magnetic fields to drive bead rotation (Fig. 1a). The current wires, each having a cross-section of 3 μm × 0.35 μm, are isolated from each other and from the fluid by a 0.5 μm thick silicon nitride layer. Every chip contains 64 wire crossings. An experiment is performed at a two-wire crossing on the chip by powering the two wires with alternating currents that are 90° out of phase. The two currents induce a rotating magnetic field at angular frequency ω_f above the area where the two wires cross each other (Fig. 1b). Currents were used between 0 and 100 mA. These were verified to generate a local temperature rise of less than 10 °C. To obtain a rotating field with constant amplitude (typically a few milliTesla) at the position of the bead, the currents are balanced to correct for the spacing between the wires and the frequency-dependent impedance. Field rotation frequencies between 0.1 Hz and 3 MHz can be achieved, limited at high frequencies by the impedance of the electrical system.

In every experiment only a single superparamagnetic bead was confined above the interception of the wires in the magnetic potential well generated by the current (van Ommering et al., 2006; Janssen et al., 2008). Due to the magnetic field gradient, the bead is pulled toward the wire and is in mild contact with the chip surface. To avoid hydrodynamic and/or magnetic interaction between beads, care was taken that beads under investigation were at least 100 μm away from a closest neighbour. Bead rotation was imaged using an optical microscope equipped with a high speed camera. It appears that the image of every bead has a characteristic pattern that allows the measurement of angular displacement using a 2D cross-correlation technique. In this image analysis technique, each frame of the movie is transformed from Cartesian to polar coordinates around the center of the bead. Each frame is then cross-correlated with rotated versions of the first bead image. The maximum in the correlation function yields the mutual rotation angle between two images. In this way the angular orientation of the bead was determined as a function of time. The bead angular rotation frequency, ω_b, was determined as an average over 20 revolutions.

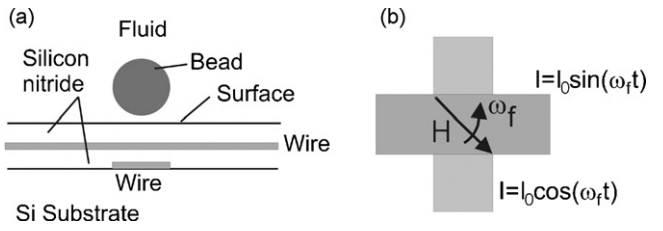

Fig. 1. (a) Cross section of the chip with current wires, each 3 μm wide and 0.3 μm thick. The magnetic bead is suspended in fluid and placed on the chip surface. (b) Top view of the crossed wires. The currents through the two wires are 90° out of phase, creating a rotating magnetic field at the position of the magnetic bead.

3. Results

3.1. Low frequency actuation

We measured the average angular rotation frequency of a bead for various field strengths, as function of the applied field frequency, see Fig. 2. The data show that the bead rotation frequency is proportional to the applied field frequency up to a so-called breakdown frequency, where a sharp drop of the bead rotation frequency is observed. Interestingly this breakdown frequency scales linearly with the applied magnetic field (inset of Fig. 2).

To understand these results, we need to consider the two torques acting on the bead: a magnetic torque driving the bead and a hydrodynamic torque counteracting the rotation. The magnitude of the magnetic torque $|\vec{\tau}|$ on a magnetic moment $\vec{m}$ placed in a magnetic field $\vec{B}$ is given by

$$|\vec{\tau}| = |\vec{m} \times \vec{B}| = mB \sin\theta. \quad (1)$$

At the breakdown frequency a maximum bead rotation frequency is observed, so at that point the magnetic torque, driving the rotation, is maximum and equal to $|\vec{\tau}| = mB$. The fact that a linear relationship is observed between the breakdown frequency and the applied field indicates that the magnetic moment is independent of the magnitude of the applied field, i.e. that in this frequency range the torque is caused by a field independent magnetic moment in the bead. Apparently, part of the magnetic material inside the bead is not able to align instantaneously its magnetic moment with the applied field and can be considered as permanent on the timescale of the experiment. Using this approximation, the magnitude of the permanent magnetic moment of the bead can be determined from the data. Let us assume a bead with a radius R, rotating at a frequency ω_b, placed in a field rotating at frequency ω_f, in a fluid with dynamic viscosity η. We introduce the angular orientation of the bead φ_b, the hydrodynamic drag constant λ and neglect the inertial forces. The equation of motion for rotation due to the permanent moment m_{perm} becomes:

$$m_{perm}\mu_0 H \sin(\omega_f t - \varphi_b) = \lambda \frac{d\varphi_b}{dt}. \quad (2)$$

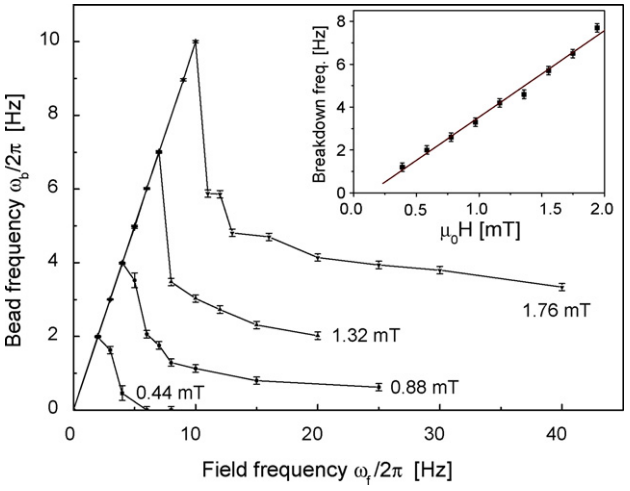

Fig. 2. Frequency response of a single magnetic bead measured at different values of the applied field, showing the occurrence of the breakdown behavior. The lines are guides to the eye. Inset: a systematic study of the breakdown frequency versus the applied field (measured on another bead).

The permanent magnetic moment can be derived from fitting the breakdown frequency as function of the applied field using:

$$m_{\mathrm{perm}} = \frac{2\pi\lambda\omega_{\mathrm{breakdown}}}{B} \quad (3)$$

Due to the close proximity of the bead to a surface, the hydrodynamic drag constant is expected to be somewhat higher than the hydrodynamic drag on a bead in a bulk fluid. We can estimate a lower limit of the magnetic moment by using the drag constant for a bead in a bulk fluid ($\lambda = 8\pi\eta R^3$). Using $\eta = 1 \times 10^{-3}$ Pa s and $R = 1.4$ μm, a permanent magnetic moment of 2.5 10^{-15} A m^2 is calculated from the fitted breakdown frequency (inset Fig. 2) This corresponds to about 1% of the saturation magnetic moment of the bead. We have characterized a number of beads and observed a variation of about a factor of 5 in the permanent moment.

Note that magnetization curves obtained by vibrating sample magnetometry (VSM) show no coercivity or remanence, see for example Fonnum et al. (2005). One might conclude that the beads have no permanent magnetic moment. However, VSM measurements can only be done with a substantial amount of magnetic material. Fonnum et al. (2005) used a powder containing many beads. Due to random orientations of the beads and the small size of the permanent magnetic moment (about 1% of the saturation magnetization), the permanent moments of the particles are not visible in VSM measurements.

Using the found permanent magnetic moment, Eq. (2) was numerically solved and used to fit the measured data (Fig. 3). The angular orientation as a function of time is plotted in the inset of Fig. 3. For frequencies below the breakdown frequency, the bead shows a constant increase of angular orientation over time (Fig. 3, case A). The increase in magnetic torque necessary for the bead to follow a higher field frequency can only be obtained if the angle between the magnetic moment and the field increases. At the breakdown frequency this angle has reached 90°, resulting in a maximum torque and therefore maximum bead frequency (Fig. 3, case B). If a field frequency above the breakdown frequency is applied (Fig. 3, case C), the bead follows the rotating field only for a short time. Due to the difference in rotation rate between the field and the bead, the bead starts lagging behind and the angle between the field and the magnetic moment increases. When the angle becomes larger than 90°, the bead slows down. Once the angle exceeds 180°, the bead starts to rotate in the opposite direction.

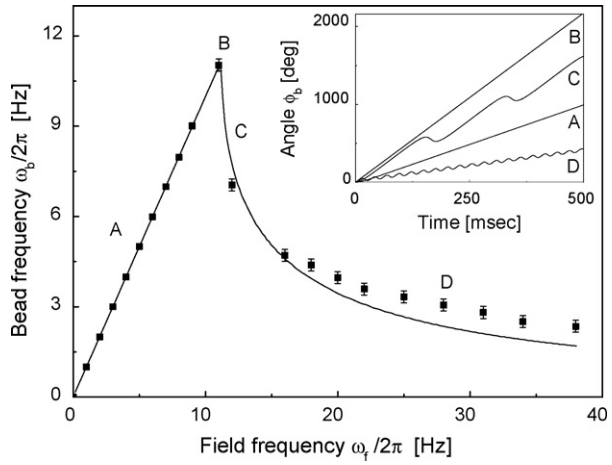

Fig. 3. The frequency at which the bead rotates versus the field frequency. The data points are fitted with the model based on a permanent magnetic moment of the bead. Inset: the simulated angular orientation of the bead versus time for different field frequencies. The letters A–D correspond to field frequencies indicated in the main panel.

The angle between the field and the moment decreases rapidly, up to the point when the moment is caught up by the field and the cycle restarts. For higher frequencies, the asymmetry between the clockwise and counterclockwise rotation becomes smaller causing the net bead frequency to decrease (Fig. 3, case D). In the recorded movies indeed phases of clockwise and counterclockwise rotation are observed upon excitation above the breakdown frequency.

There are three indications that the low-frequency rotation is caused by a permanent magnetic moment with a fixed orientation and not by an inhomogeneous spatial distribution of the nanoparticles inside the bead. First, the measured breakdown frequency increases linearly rather than quadratically with the applied field (inset of Fig. 2). Second, we observed in the microscope that every bead orientates itself in a unique direction with respect to an applied field. Finally we observed for field frequencies slightly above the breakdown frequency that the rotation is periodically interrupted by short phases of counter-rotation. These phases appear at a frequency $\omega = \omega_f - \omega_b$. If the orientation of the magnetic moment would be able to flip 180° along an easy axis, the phases of counter-rotation would appear at twice that frequency.

The model based on a permanent magnetic moment fits the measured frequency response of the bead, but for increasing field frequency, the measured bead rotation frequency decreases slower than the simulated bead rotation frequency (Fig. 3). It is observed that this deviation becomes larger not only for increasing field frequency, but especially for increasing field strength.

3.2. High frequency actuation

Fig. 4a shows the bead rotation frequency for two different field amplitudes at rotation frequencies of the applied magnetic field ranging from 0.1 Hz to 3 MHz. To our surprise, the bead rotation frequency increases for applied field frequencies between approximately 100 Hz and 400 kHz and decreases again for even higher field frequencies. This behavior at high field frequencies cannot be explained by the model based on the permanent magnetic moment. Apparently for low and high field frequencies two different physical mechanisms dictate the bead rotation behavior.

The physical mechanism underlying the increase in bead rotation frequency at high field frequencies was investigated by studying the dependence on the field amplitude. At frequencies above 100 Hz we found a quadratic increase in bead rotation frequency with increasing field strength (Fig. 4b). This indicates that the torque is caused by a field-induced magnetization. The observation of a torque implies that in the high frequency range, the magnetization is not able to follow the field instantaneously.

The phase lag can be derived from the magnetic relaxation time τ_m of an iron oxide nanoparticle in an external field with magnetic flux density B: $\tau_m = \nu_0^{-1} \exp((KV \pm \mu B)/k_B T)$, with ν_0 the attempt frequency, K the magnetic anisotropy constant, V the volume of the ironoxide nanoparticle, μ the magnetic dipole moment of the nanoparticle and k_B the Boltzmann constant. For nanoparticles made of magnetite and an applied magnetic flux density of ~1 mT, $KV/\mu B \cong 36$, so that the anisotropy energy KV dominates the magnetic relaxation time.

3.3. Induced magnetic moment

The phase lag of the ensemble of nanoparticles in the bead is described using a frequency dependent imaginary susceptibility (Fannin et al., 2006) that contains the magnetic relaxation time. The frequency dependent magnetization M of a bead can be expressed as a complex vector $\vec{M}(\omega_f) = (\chi'(\omega_f) - i\chi''(\omega_f))\vec{H}$. The torque density, $\vec{\tau}$, on the bead equals the cross product of the magnetization

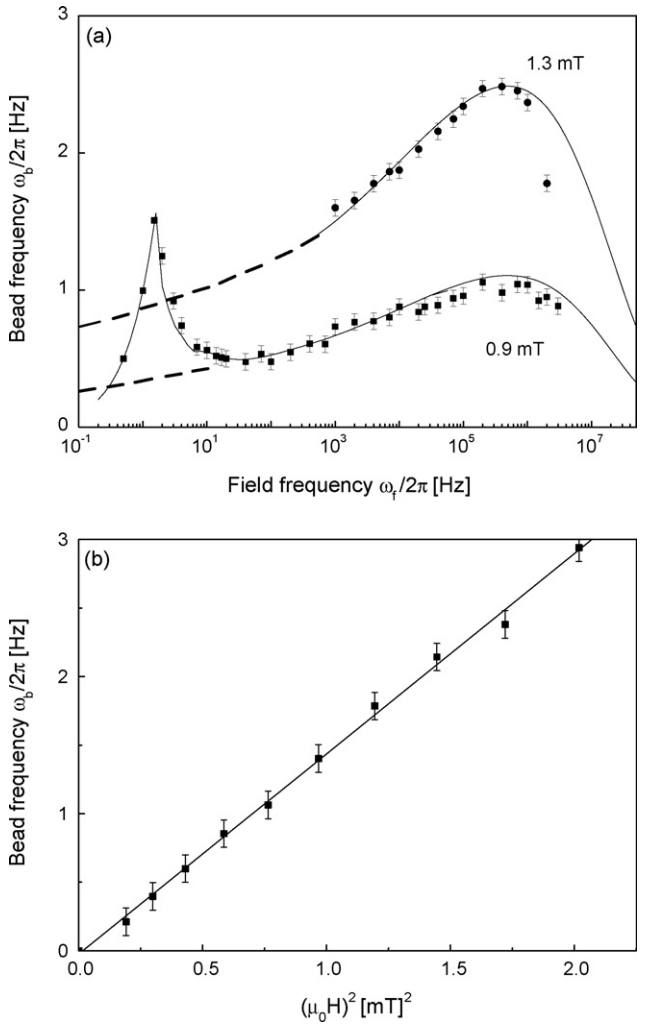

Fig. 4. (a) Frequency response of a magnetic bead measured at two different values of the applied field. The two data sets are fitted using Eqs. (2) and (6). The only difference between the two curves is the magnitude of the applied magnetic field. The dashed lines represent the low-frequency behavior in the absence of a permanent moment in the bead [using Eq. (2) rather than Eq. (6)]. (b) The observed bead rotation frequency at a field frequency of 40 kHz versus the square of the field strength.

and field:

$$\vec{\tau} = \vec{M} \times \mu_0 \vec{H} = \mathrm{Re}[\chi(\omega_\mathrm{f})\vec{H}] \times \mu_0 \vec{H} = \chi''(\omega_\mathrm{f})\mu_0 H^2 \vec{e}_{\omega_\mathrm{f}}, \quad (4)$$

with H the amplitude and $\vec{e}_{\omega_\mathrm{f}}$ the unit vector of the rotating field. Note that the torque is proportional to the square of the applied field and to the imaginary part of the susceptibility. The magnetization caused by the real part of the susceptibility is parallel to the applied field and does therefore not contribute to the torque, whereas the magnetization caused by the imaginary part of the susceptibility does contribute to the torque because it is perpendicular to the applied field.

For monodisperse nanoparticles the imaginary part of the susceptibility equals $\chi''(\omega_\mathrm{f}) = \chi_0 \frac{\omega_\mathrm{f}\tau_\mathrm{m}}{1+\omega_\mathrm{f}^2\tau_\mathrm{m}^2}$ with χ_0 the susceptibility of the nanoparticle material at static field. To calculate the torque on a bead, it is important to include the fact that the bead contains a distribution of ironoxide nanoparticles with different sizes and thus different relaxation times. Neither the number of nanoparticles inside a bead nor the size distribution is given by the manufacturer of the beads. We therefore modeled the resulting imaginary susceptibility by using a log-normal nanoparticle size distribution, which is commonly observed in the synthesis of magnetic particles (Johansson et al., 1997). The distribution is divided in n size intervals, each with a total nanoparticle volume V_n. Each interval contributes to the total susceptibility with weight factor V_n^2 (Rosensweig, 1985). The total imaginary susceptibility of the bead becomes:

$$\chi''(\omega_\mathrm{f}) = \frac{\chi_\mathrm{bead}}{\sum_n V_n^2} \sum_n \frac{\omega_\mathrm{f}\tau_{\mathrm{m},n}}{1+\omega_\mathrm{f}^2\tau_{\mathrm{m},n}^2} \cdot V_n^2 \quad (5)$$

where we normalized the complex susceptibility to the bead susceptibility χ_bead at static field.

The torque due to the induced magnetic moment is added to the equation of motion (Eq. (2)) resulting in

$$m_\mathrm{perm}\mu_0 H \sin(\omega_\mathrm{f} t - \varphi_\mathrm{b}) + \chi''(\omega_\mathrm{f})\mu_0 H^2 V = \lambda \frac{\mathrm{d}\varphi_\mathrm{b}}{\mathrm{d}t} \quad (6)$$

with V the volume of the magnetic content of the bead. Here we make the approximation that the magnetic moments of the nanoparticles effectively sum to a single dipole moment of the bead.

Using Eqs. (5) and (6), we can fit the measured bead rotation frequency assuming an anisotropy constant K of 5×10^4 J/m^3 (Bødker et al., 1994), χ_0 of 0.64 and a log-normal distribution with a mean nanoparticle radius r_m of 3.8 nm (Fonnum et al., 2005) and a standard deviation σ of 0.26. It appears that the position of the peak at high frequencies is primarily determined by the anisotropy constant and the mean nanoparticle radius, while the width and shape of the peak are mainly determined by the standard deviation σ. The physical model is validated by fitting the frequency curve for a single bead at two different strengths of the applied field, using the same set of parameters for the magnetic bead (Fig. 4a). Since the fit in Fig. 4a does not yield a unique set of parameters, this technique cannot be used for determining the magnetic properties of the beads in detail. Nevertheless the model reveals the mechanism behind the generation of torque on the bead at high field frequencies.

It is interesting to note that a qualitative analogue exists of the phenomena observed here. A nanowire placed in a high-frequency rotating electric field rotates at a frequency much lower than the applied field frequency (Fan et al., 2005). In that case the torque has an electric origin, generated by the interaction between an applied electric field and a field-induced electric dipole moment. In our case the torque results from the interaction between an applied magnetic field and a field-induced magnetic moment.

Our model correctly accounts for the observed decrease of the bead rotation frequency beyond 400 kHz. We understand this as follows. At each field frequency, a different part of the nanoparticle size distribution contributes to the torque. Nanoparticles with a relaxation time comparable to $2\pi/\omega_\mathrm{f}$ follow the field with a certain phase lag, causing the imaginary part of the magnetization. Nanoparticles that have a fast relaxation time ($\tau_\mathrm{m} \ll 2\pi/\omega_\mathrm{f}$) follow the field instantaneously, giving the real part of the magnetization. Finally, large nanoparticles with a high relaxation time ($\tau_\mathrm{m} \gg 2\pi/\omega_\mathrm{f}$) do not respond to the field. The observed maximum response is caused by the fact that at frequencies above one MHz, even the smallest nanoparticles cannot follow the high field frequency and the rotation frequency of the bead goes to zero.

4. Outlook to future work

We expect that the demonstrated quantitative control of torque and rotation will generate a wide range of novel functionalities in bead-based biosensors. The basic approach is that the measurement of rotation and torque properties gives information about captured biological molecules, their bindings, and their function. We aim to use torsion information to probe molecules and to make distinctions between different binding modalities, e.g. single-

bond versus double-bond binding, weak binding versus strong binding, and specific versus non-specific binding. Torsion-based single-molecule experiments have demonstrated novel types of assays, e.g. revealing the activity of DNA repair enzymes (Besteman et al., 2007; Koster et al., 2007). We will study torsion-based protein assays as well as nucleic-acid assays, measuring for example the torsional stiffness of the captured molecules and the torsion-driven rupture of biological bonds. Note that the magnetic moments measured in this paper appear to be of the order of 10^{-15} A m^2. This implies that a rotating magnetic field of a few milliTesla can easily inject an energy of several tens of kJ/mol into a biological bond, which is of the same order as the energy of the strongest known antibody–antigen bonds like biotin–streptavidin (Panhorst et al., 2005). Finally, we note that the magnetic field generated by on-chip current wires has a strong dependence on distance to the wire. In a biological experiment, the distance between a bead and the surface depends on the system under study, e.g. several nanometers for an antibody–antigen couple up to several micrometers for long DNA strands. We will investigate alternative magnetic designs for assays in which more homogenous magnetic fields are preferred, e.g. designs with magnetic field sources that have larger dimensions than the on-chip current wires of the present study.

5. Conclusion

In summary, we have demonstrated rotation of magnetic beads in a rotating magnetic field over a wide range of applied field frequencies. At low field frequencies, the torque is determined by a small permanent magnetic moment in the bead of the order of 10^{-15} A m^2. At high field frequencies, the phase lag between the field and the induced magnetization gives rise to a torque on the bead. The torque can be understood from the non-zero relaxation time of the ironoxide nanoparticles in the bead and can be quantitatively described with a frequency dependent complex susceptibility. In conclusion, our technique represents a novel way to quantitatively determine the magnetic torque of single magnetic beads in a rotating magnetic field.

References

Astalan, A.P., Ahrentorp, F., Johansson, C., Larsson, K., Krozer, A., 2004. Biosens. Bioelectron. 19, 945–951.

Aytur, T., Foley, J., Anwar, M., Boser, B., Harris, E., Beatty, P.R., 2006. J. Immunol. Methods 314 (1/2), 21–29.

Baselt, D.R., Lee, G.U., Natesan, M., Metzger, S.W., Sheehan, P.E., Colton, R.J., 1998. Biosens. Bioelectron. 13, 731–739.

Besse, P.A., Boero, G., Demierre, M., Pott, V., Popovic, R., 2002. Appl. Phys. Lett. 80 (22), 4199–4201.

Besteman, K., Hage, S., Dekker, N.H., Lemay, S.G., 2007. Phys. Rev. Lett. 98, 058103.

Bødker, F., Mørup, S., Linderoth, S., 1994. Phys. Rev. Lett. 72, 282–285.

de Boer, B.M., Kahlman, J.A.H.M., Jansen, T.P.G.H., Duric, H., Veen, J., 2007. Biosens. Bioelectron. 22 (9/10), 2366–2370.

Cohen-Tannoudji, L., Bertrand, E., Baudry, J., Robic, C., Goubault, C., Pellissier, M., Johner, A., Thalmann, F., Lee, N.K., Marques, C.M., Bibette, J., 2008. Phys. Rev. Lett. 100, 108301.

Ejsing, L., Hansen, M.F., Menon, A.K., Ferreira, H.A., Graham, D.L., Freitas, P.P., 2004. Appl. Phys. Lett. 84 (23).

Ejsing, L., Hansen, M.F., Menon, A.K., Ferreira, H.A., Graham, D.L., Freitas, P.P., 2005. J. Magn. Magn. Mater. 293 (1), 677–684.

Fannin, P.C., Cohen-Tannoudji, L., Bertrand, E., Giannitsis, A.T., Mac Oireachtaigh, C., Bibette, J., 2006. J. Magn. Magn. Mater. 303, 147–152.

Fan, D.L., Zhu, Q., Cammarata, R.C., Chien, C.L., 2005. Phys. Rev. Lett. 94, 247208.

Fonnum, G., Johansson, C., Molteberg, A., Mørup, S., Aksnes, E., 2005. J. Magn. Magn. Mater. 293, 41–47.

Fukumoto, H., Takeguchi, K., Nomura, M., Endo, H., 2005. Solid State Sens., Actuators Microsyst. 2, 1780–1783.

Janssen, X.J.A., van Ijzendoorn, L.J., Prins, M.W.J., 2008. Biosens. Bioelectron. 23, 833–837.

Johansson, C., Hanson, M., Pedersen, M.S., Mørup, S., 1997. J. Magn. Magn. Mater. 173, 5–14.

Koster, D.A., Palle, K., Bot, E.S.M., Bjornsti, M., Dekker, N.H., 2007. Nature 448, 213–217.

Kurlyandskaya, G.V., Sánchez, M.L., Hernado, B., Prida, V.M., Gorria, P., Tejedor, M., 2003. Appl. Phys. Lett. 82 (18).

Megens, M., de Theije, F., de Boer, B., van Gaal, F., 2007. J. Appl. Phys. 102, 014507.

Mornet, S., Vasseur, S., Grasset, F., Duguet, E., 2004. J. Mater. Chem. 14, 2161–2175.

Morozova, T.Y., Morozov, V.N., 2008. Anal. Biochem. 374, 263–271.

Mulvaney, S.P., Cole, C.L., Kniller, M.D., Malito, M., Tamanaha, C.R., Rife, J.C., Stanton, M.W., Whitman, L.J., 2007. Biosens. Bioelectron. 23, 191–200.

Nikitin, P.I., Vetoshko, P.M., Ksenevich, T.I., 2007. J. Magn. Magn. Mater. 311 (1), 445–449.

van Ommering, K., Nieuwenhuis, J.H., van IJzendoorn, L.J., Koopmans, B., Prins, M.W.J., 2006. Appl. Phys. Lett. 89, 142511.

Panhorst, M., Kamp, P.B., Reiss, G., Brückl, H., 2005. Biosens. Bioelectron. 20, 1685–1689.

Pollert, E., Knížek, K., Maryško, M., Kašpar, P., Vasseur, S., Duguet, E., 2007. J. Magn. Magn. Mater. 316 (2), 122–125.

Prins, M.W.J., Megens, M., 2007. In: Buschow, et al. (Eds.), Chapter in Encyclopedia of Materials: Science and Technology. Elsevier, pp. 1–6, doi:10.1016/B978-008043152-9/02146-1.

Rife, J.C., Miller, M.M., Sheehan, P.E., Tamanaha, C.R., Tondra, M., Whitman, L.J., 2003. Sens. Actuators A: Phys. 107 (3), 209–218.

Rosensweig, R.E., 1985. Ferrohydrodynamics. Cambridge University Press.

Wild, D., 2005. The Immunoassay Handbook, 3rd ed. Elsevier.

Wirix-Speetjens, R., Fyen, W., De Boeck, J., Borghs, G., 2006. J. Appl. Phys. 99, 103903-1–103903-4.